FED-Vol. 118, Liquid Solid Flows
ASME 1991

FINITE SIZE EFFECTS IN FLUIDIZED BEDS

P. Singh and D. D. Joseph
Department of Aerospace Engineering and Mechanics
University of Minnesota
Minneapolis, Minnesota

ABSTRACT

We consider a one-dimensional theory of fluidized beds in which the fluids and solids equations are decoupled and the system is closed with a momentum equation for the particles alone. The simplest theory, based on the Foscolo-Gibilaro force law, is used except that the force that the fluid exerts on the solid is assumed to depend on the area fraction rather than the volume fraction of solids and the gradient of the volume fraction which expresses the particle phase pressure is put to zero. The area and volume fraction are related by a simple geometrical construction in the case of fluidization of a monodisperse suspension of spheres of radius R, taking into account the area of intersection of these spheres with a plane perpendicular to the flow. Our one-dimensional theory then has three unknowns, the volume fraction, the area fraction and the particle velocity, rather than two. The two-variable theory is recovered in the limit R→0. These equations admit uniform fluidization as a solution which is Hadamard unstable in the two-variable theory but simply unstable in the three-variable theory, with a distinguished set of marginally stable modes belonging to a countable set of blocked wave numbers generated by the relation between the volume and area fraction. The blockage function regularizes the ill-posed problem and generates a structured dynamical response with a set of discrete stationary marginal modes. The initial value problem for our three-variable, one-dimensional theory is solved by numerical methods for periodic boundary and different initial conditions. No solutions of permanent form with discrete spectral peaks were found. Instead, we found chaotic solutions with nearly stationary levels of the power when a certain dimensionless "growth rate" parameter is below a critical value and unstable solutions whose power levels increase without bound when this value is above the critical one. The power spectrum of a bounded solution is continuous and is such that the power level is very low for wave numbers in the blocked set which are marginally stable in the linear theory. We made video recordings of experiments on beds of fluidized spheres confined to move in two dimensions between glass plates. Analysis of the digitized signals gives the area fraction as a function of space and time at a discrete set of points. The temporal autocorrelation of the area fraction at a point decays to zero at all Reynolds numbers, as in a chaotic response. The spatial autocorrelation becomes negative and then goes to zero for large spatial shifts. Analysis of chaotic and dispersive wavelike structures is carried out by plotting the level lines of two-dimensional continuous power spectra depending on a frequency and wave number. The waves of highest power move to higher frequencies as the Reynolds number is increased. The amplitude of the measured spectra is a strong function of frequency and wave number with deep minima at the blocked wave numbers predicted by stability theory and the numerical integration of the initial value problem. At low Reynolds numbers, the measured spectrum looks like the growth rate function from linear theory. As the Reynolds number increases, the graph of the power spectrum gets higher energy at smaller wave numbers, consistent with the increasing importance of wake effects. We think that our simple theory with finite size but no gradient effects is in astonishing agreement with experiments.

1. INTRODUCTION

We are going to let our extended abstract replace one part of this introduction. Actually there are two papers which precede this one, both by Singh and Joseph, [1990] and [1991]. Other papers which bear upon the general topic of fluidization relevant to our work are discussed in the introduction of the two previous papers and they will not be mentioned again here. It will perhaps suffice to motivate this omission by saying that the derivation of finite size effects in the theory and most of the features of the analysis of theory and experiments are discussed only in the two aforementioned papers and in this one. Our view of our theory has undergone a slow evolution and the version presented here is more clearly motivated and easily understood than the previous versions.

2. TWO-VARIABLE AND THREE-VARIABLE THEORIES WITHOUT GRADIENTS

The theories which we consider here are one-dimensional particle-in-a-bed theories of three-dimensional fluidization in which the effects of variations of fields on the planes perpendicular to flow are presumed to be adequately represented on the average. The words "particle in a bed" mean that the momentum balance for the fluid and solid phases is decoupled in the sense that it is possible *a priori* to model the effects of fluid on the particles. In this case we get a two-variable, one-dimensional theory of the type proposed by Foscolo and Gibilaro [1987] for the solids fraction Φ and the particle velocity u. The solids fraction satisfies a conservation law

$$\frac{\partial \Phi}{\partial t} + \frac{\partial (u\Phi)}{\partial z} = 0 \qquad (2.1)$$

where z is in the direction of the fluidizing velocity u_c. The momentum equation for the particles is framed in terms of the force

$$F(u,\Phi) = m\tilde{g}\left\{-(1-\Phi) + \left[\frac{u_c-u}{U(0)}\right]^{\frac{4.8}{n}}(1-\Phi)^{-3.8}\right\} \tag{2.2}$$

on a single one of them. Here m is the mass of a single sphere of radius R, $\tilde{g}=(\rho-\rho_f)g/\rho$ is reduced gravity, ρ is the density of the sphere, ρ_f is the density of the fluid, $U(\Phi)$ is the steady fall velocity under gravity of a sphere in a uniform dispersion of spheres of solids fraction Φ. In a uniform dispersion u=0 and Φ is independent of z. The fluidization velocity $u_c=u_f(1-\Phi)-u\Phi$, where u_f is the fluid velocity, is in general solenoidal, independent of z, and when u=0, u_c satisfies the Richardson and Zaki correlation

$$u_c = U(\Phi) = U(0)\,(1-\Phi) \tag{2.3}$$

U(0) is the velocity of one sphere in a pure liquid and it can be expressed in terms of the Reynolds number using various empirical correlations and n(Re) is the Richardson and Zaki exponent; it lies between 4.8 for small Reynolds numbers $Re = \frac{u_c 2R}{\nu}$ and 2.4 for large Re. The ingenious force law (1.2) was invented by Foscolo and Gibilaro (see the [1987] paper for earlier references) but it cannot be regarded as established.

The momentum equation of Foscolo and Gibilaro can be expressed as

$$mN\left(\frac{\partial u}{\partial t} + u\frac{\partial u}{\partial z}\right) = F + \frac{4}{3}R\frac{\partial F}{\partial \Phi}\frac{\partial \Phi}{\partial z} \tag{2.4}$$

where

$$F = NF \tag{2.5}$$

and

$$N = \frac{\rho}{m}\Phi = \Phi \Big/ \frac{4}{3}\pi R^3 \tag{2.6}$$

is the number density.

Equations (2.1) and (2.4) are then a system of one-dimensional equations in two variables Φ and u. The last term of (2.4) which involves a derivative of Φ can be said to express the pressure of the particle phase. This type of system has also been developed by Batchelor [1988] and the gradient term interpreted there is in terms of diffusion against the gradient of concentration in which empty places tend to fill up as an effect of small fluctuations of particle velocity analogous to Brownian motions. To have diffusion against the gradient the sign of the last term in (2.4) must be positive. Uniform fluidization with a constant $\Phi=\Phi_0$ and u=0 is a solution of (2.2) and (2.4) and it is Hadamard unstable if the gradient terms in (2.4) are neglected. The gradient term can regularize this instability and even introduce regions in the space of parameters where the uniform state is stable. In this case the criterion for the loss of stability is independent of the wave number of the perturbation, so if the system is unstable at all, it is unstable to long waves as well as short waves. Batchelor also has a viscosity term which stabilizes short waves but does not change the stability criterion.

Central to our three-variable theory is a little construction which relates the volume fraction Φ of solids to the area fraction. Consider a plane at z. Locate the origin of a coordinate x on z. Spheres at a distance $|x|<R$ from z intersect z, and their area of intersection is $\pi(R^2-x^2)$. If N(x+z,t) is the number density of spheres with centers at x+z, then N(x+z,t)Adx is the number of such spheres in an infinitesimal volume Adx, where A is the area of, say, some square $A=L^2$ with a very large L. The area A_S on the plane which is cut out by spheres is obtained by summing all of the areas of intersections coming from infinitesimal volumes centered on x+z as x varies from –R to R.

$$A_S = \int_{-R}^{R} N(x+z,t)\pi(R^2-x^2)\,Adx \tag{2.7}$$

After writing $A_S/A=\phi$, using (2.6), we get

$$\phi = \frac{3}{4R^3}\int_{-R}^{R}\Phi(x+z,t)\,(R^2-x^2)\,dx\,. \tag{2.8}$$

When Φ is independent of x, then

$$\phi(z,t) = \Phi(z,t)\,. \tag{2.9}$$

Equation (2.9) holds approximately when R is small. This shows that the three-variable theory reduces to the two-variable theory when R is small.

The next step in the construction of the three-variable theory is to replace the volume fraction Φ in the Richardson and Zaki correlation (2.3) and in the force law (2.2) with the area fraction ϕ. This step is taken because it leads to a good result. The nonlinear three-variable theory without gradients is given by

$$\frac{\partial \Phi}{\partial t} + \frac{\partial(u\Phi)}{\partial z} = 0 \tag{2.10}$$

$$\phi = \frac{3}{4R^3}\int_{-R}^{R}\Phi(x+z,t)\,(R^2-x^2)\,dx\,. \tag{2.11}$$

$$\frac{\partial u}{\partial t} + u\frac{\partial u}{\partial z} = \tilde{g}\left\{-\varepsilon + \left[\frac{u_c-u}{U(0)}\right]^{\frac{4.8}{n}}\varepsilon^{-3.8}\right\} \tag{2.12}$$

where $\varepsilon=1-\phi$ and the composite velocity u_c, which is the constant superficial velocity at the inlet of the bed is given by

$$u_c = U(0)\varepsilon_0^n \tag{2.13}$$

in uniform fluidization when u=0, $\Phi=\Phi_0$ and $\phi=\phi_0$. Obviously uniform fluidization is a solution of this system of equations.

3. STABILITY OF UNIFORM FLUIDIZATION AND THE BLOCKAGE FUNCTION

We now linearize equations (2.10), (2.11) and (2.12) at the solution $(u,\Phi,\phi)=(0,\Phi_0,\phi_0)$ and find that the system of perturbed equations, denoted by the subscript 1, is

$$\frac{\partial \Phi_1}{\partial t} + \Phi_0\frac{\partial u_1}{\partial z} = 0\,, \tag{3.1}$$

$$\phi_1 = -\varepsilon_1 = \frac{3}{4R^3}\int_{-R}^{R}\Phi_1(z+x,t)\,(R^2-x^2)\,dx\,, \tag{3.2}$$

$$\frac{\partial u_1}{\partial t} = -\hat{a}u_1 - \hat{b}\varepsilon_1\,, \tag{3.3}$$

where

$$\hat{a} = \frac{4.8\tilde{g}}{nU(0)}\,\epsilon_0^{1-n}, \tag{3.4}$$

$$\hat{b} = 4.8\tilde{g}. \tag{3.5}$$

After eliminating ϵ_1 and u_1 from (3.1), (3.2), and (3.3), we find a single second order equation

$$\frac{\partial^2\Phi_1}{\partial t^2} = -\hat{a}\frac{\partial\Phi_1}{\partial t} - \hat{b}\Phi_0\frac{3}{4R^3}\frac{\partial}{\partial z}\int_{-R}^{R}\Phi_1(z+x,t)(R^2-x^2)dx. \tag{3.6}$$

The stability of uniform fluidization may be determined by analysis of (3.6) using normal modes.

$$\Phi_1 = \hat{\Phi}_1\, e^{\sigma t}\, e^{i\alpha z}.$$

We obtain a complex dispersion relation of the form

$$\sigma^2 + \sigma\hat{a} + i\alpha\hat{b}\,\Phi_0\Theta(\alpha R) = 0. \tag{3.7}$$

where

$$\Theta(\alpha R) = 3\left[\frac{\sin\alpha R}{(\alpha R)^3} - \frac{\cos\alpha R}{(\alpha R)^2}\right] \tag{3.8}$$

is the blockage function. We may solve this quadratic equation for

$$\sigma = -\frac{\hat{a}}{2} \pm \frac{\hat{a}}{2}\sqrt{1 - i\,\Sigma} \tag{3.9}$$

where

$$\Sigma = -\frac{4\alpha\hat{b}\,\phi_0\Theta(\alpha R)}{\hat{a}^2} \tag{3.10}$$

We wish to draw the readers attention to the importance of the blockage function $\Theta(\alpha R)$. The graph of $\Theta(\alpha R)$ versus $2\alpha R$ is shown in figure 1. The zeros of $\Theta(\alpha R)$ are at $\alpha = \frac{4.493}{R}, \frac{7.7253}{R}, \frac{10.904}{R}, \ldots$ The blockage function tends to zero for large values of α like $\frac{1}{\alpha R^2}$.

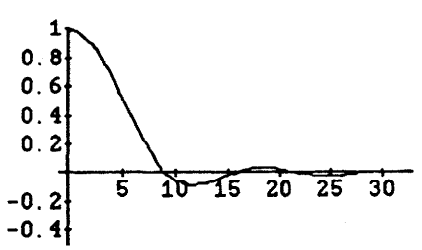

Fig. 1. $\Theta(\alpha D)$ is plotted as a function of αD.

First consider the limit α fixed, however large, $R \to 0$. In this limit

$$\alpha\,\Theta(\alpha R) \to \alpha.$$

Now let $\alpha \to \infty$ for short waves. A little analysis shows that

$$\mathrm{re}\,\sigma \to \sqrt{\hat{b}\phi_0}\sqrt{\alpha}.$$

Hence re $\sigma \to \infty$ as $\alpha \to \infty$ and the uniform state of fluidization is Hadamard unstable. On the other hand for R>0, since $\alpha\Theta(\alpha R) \to 0$ as $\alpha \to \infty$, the blockage function regularizes the Hadamard instability (see figure 2). Now suppose R>0 is fixed. Then at each and every zero of $\alpha\Theta(\alpha R)$ we have

$$\sigma = 0 \text{ or } -\hat{a},$$

otherwise

$$\mathrm{re}\,\sigma > 0.$$

We may conclude then that uniform fluidization is unstable, but not Hadamard unstable when the finite size of particles is accounted for in the calculation of the area fraction. We also note that there is a blockage of waves of wave length $\frac{2\pi}{\alpha}$ for $\alpha = 0$, $\frac{4.493}{R}$, etc. which are neutrally stable.

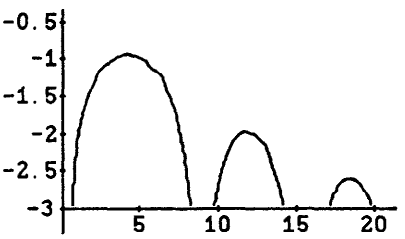

Fig. 2. re $\sigma(\alpha D)$ is plotted as a function of αD.

4. COMPARISON OF REGULARIZATION BY FINITE SIZE EFFECTS WITH GRADIENT REGULARIZATION

If finite size effects are negligible, as in the limiting case $R \to 0$, $\Theta(\alpha R) \to \Theta(0) = 1$, and gradient terms are included, we get a two variable theory. We linearize (2.1) and (2.4) around the uniform fluidization. The linearized equations are (3.1) and

$$\frac{\partial u_1}{\partial t} = -\hat{a}u_1 - \hat{b}\epsilon_1 - \hat{c}\frac{\partial\epsilon_1}{\partial z}. \tag{4.1}$$

The dispersion relation for the system is given by

$$\sigma^2 + \sigma\hat{a} + (\alpha^2\hat{c} + i\alpha\hat{b})\,\Phi_0 = 0 \tag{4.2}$$

where $\hat{c} = \frac{2}{3}D\hat{b}$ is the coefficient of elasticity and it is positive. So

$$\sigma = -\frac{\hat{a}}{2} \pm \sqrt{\frac{\hat{a}^2}{4} - \alpha^2\hat{c} - i\alpha\hat{b}}$$

Since $\hat{c}$ is positive, the short waves are stabilized but the dependence of σ on α is rather flat with one zero at most, unlike (3.9). Some choices of the coefficients of the gradient terms in (4.1) lead to regions of stability of uniform fluidization. In fact they lead to the conclusion that the beds we used in our experiments are operating in regions of stable uniform fluidization. We get such stability from FG theory when: Re=300, u_c= 0.044 m/s, $\phi = 0.8$, n = 3.0, D =0.0063 m, $\frac{\rho}{\rho_f} = 1.12$, $\tilde{g} = 1.05$ m/s^2. It is difficult to use Batchelor's theory to check the stability since some of the coefficients are not known, but he says " ... $\frac{\rho}{\rho_f}$ is seldom less than 2 for a marginally stable bed." These theories disagree with our experiments and those of Volpicelli, Massimilla and Zenz [1966] in which all the flows

were decidedly not uniform. Figure 3 shows the effect of a rather large elasticity $\hat{c}$, all wave numbers are stabilized. It is quite clear from this figure that the structure due to the blockage in the wave number space is lost when the gradient terms are included.

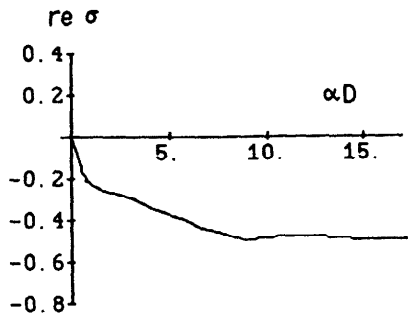

Fig. 3. re $\sigma(\alpha D)$ is plotted as a function of αD for the gradient theory (4.1), $\hat{c}$ is a non-zero positive constant.

5. NONLINEAR SATURATION OF INSTABILITY OF UNIFORM FLUIDIZATION

5.1 Dimensional analysis

The problem contains six parameters: $\Phi_0 = 1 - \varepsilon_0$ is the average solids fraction, R is the radius of particles, u_c is the superficial velocity, U(0) is the superficial velocity for $\varepsilon = 1$, n is the Richardson and Zaki exponent and $\tilde{g} = g\frac{\rho - \rho_f}{\rho}$ is a reduced gravity, where ρ, ρ_f are the densities of the solid and fluid phases. We now show that these six parameters form three non-dimensional groups. It is convenient to change the frame of reference to the one moving upwards with the velocity u_c

$$x = z - u_c t, \quad v = u - u_c.$$

So we have

$$\frac{\partial}{\partial x} = \frac{\partial}{\partial z},$$

$$\frac{\partial}{\partial t}\Big|_{x \text{ fixed}} = \frac{\partial}{\partial t}\Big|_{z \text{ fixed}} - u_c \frac{\partial}{\partial x}.$$

By substituting above expressions in (2.10), (2.11) and (2.12), and using (2.6) we get

$$\frac{\partial N(x,t)}{\partial t} + \frac{\partial [v(x,t)\, N(x,t)]}{\partial x} = 0,$$

$$mN\left(\frac{\partial v}{\partial t} + v\frac{\partial v}{\partial x}\right) =$$

$$m\tilde{g}\left\{-\varepsilon + \left[\frac{V}{U(0)}\right]^{\frac{4.8}{n}} \varepsilon^{-3.8}\right\},$$

$$\phi(x,t) = 1 - \varepsilon = \int_{-R}^{R} N(x+\xi,t)\, \pi(R^2 - \xi^2)\, d\xi. \qquad (5.1.1)$$

To find the controlling dimensionless parameters we introduce scaling parameters which are designated by *:

$$T^* = \frac{u_c}{\tilde{g}},$$

$$L^* = D = 2R,$$

$$U^* = \frac{D}{T^*} = \frac{D\tilde{g}}{u_c},$$

$$\varepsilon^* = \varepsilon_0,$$

$$N^* = \frac{\pi}{6} N_0, \qquad (5.1.2)$$

where ε_0 is the average area fraction of the fluid and N_0 is the average number density.
Let

$$N' = \frac{N}{N^*}, \quad \varepsilon' = \frac{\varepsilon}{\varepsilon^*}, \quad u' = \frac{v}{U^*},$$

$$z' = \frac{x}{L^*} \text{ and } t' = \frac{t}{T^*}, \qquad (5.1.3)$$

be dimensionless variables. We substitute these variables in (5.1.1) and obtain the following equations, which after dropping the primes (') can be written as

$$\frac{\partial N(z,t)}{\partial t} + \frac{\partial [u(z,t)\, N(z,t)]}{\partial z} = 0,$$

$$\frac{\partial u}{\partial t} + u\frac{\partial u}{\partial z} = -\varepsilon_0 \Sigma_1 \varepsilon + \varepsilon_0 \left(\frac{1}{\Sigma_1}\right)^{\frac{4.8-n}{n}} u^{\frac{4.8}{n}} \varepsilon^{-3.8},$$

$$\varepsilon = \frac{1}{\varepsilon_0} - \frac{1-\varepsilon_0}{\varepsilon_0} \int_{-0.5}^{0.5} N(z+\xi,t)\, \pi(0.5^2 - \xi^2)\, d\xi, \qquad (5.1.4)$$

where $\Sigma_1 = \frac{u_c^2}{D\tilde{g}}$. The dynamical system (5.1.3) is characterized by three parameters, Σ_1, the area fraction ε_0 of the fluid and the Richardson and Zaki exponent n, which is a function of the Reynolds number.

The maximum value Σ_m of Σ, as a function of α, is attained at $\alpha = \frac{4.2}{D}$. Using this value of α we find that $\alpha\, \Theta(\alpha R) = \frac{2.6}{D}$ and

$$\Sigma_m = \frac{2.17\, n^2\, \phi_0}{\varepsilon_0^2} \frac{u_c^2}{D\tilde{g}}$$

$$= \frac{2.17\, n^2\, \phi_0}{\varepsilon_0^2} \Sigma_1. \qquad (5.1.5)$$

From this relation we may conclude that for a given value of the area fraction of solids and n, Σ_1 completely determines Σ_m. The area fraction ϕ_0 defines an operating condition and is not a parameter which distinguishes one bed from another. The Richardson and Zaki exponent n has only a small range: it is 4.8 for very small Reynolds numbers and it is 2.4 for very large Reynolds numbers. So the most important parameter which distinguishes one fluidized bed from the other is Σ_m, for large Σ_m the maximum growth rate σ is large and for small Σ_m the maximum growth rate σ is small. The experiments described in Singh and Joseph show that there is a one to one correspondence between the growth rates given by the linearized model and the amplitudes different wave numbers attain in a steady real two-dimensional fluidized bed. Later in this section we will present the results of numerical simulations which are in harmony with these experimental observations.

5.2 Fourier-Collocation Method

We approximate u and N by

$$u(z_j,t) = \sum_{k=-l}^{l-1} \hat{u}_k(t)\, e^{ikz_j}$$

$$N(z_j,t) = \sum_{k=-l}^{l-1} \hat{N}_k(t) e^{ikz_j}$$

$$\text{for } j = 0, 1, 2, \ldots, 2l-1, \qquad (5.2.1)$$

where 2 l is the number of collocation points. The computational domain is from x = 0 to x =2π, and the collocation points are uniformly distributed. We use a staggered grid for the velocity u and the number density N. The velocities u(zj,t)'s are defined at $z_j = 0, \frac{\pi}{l}, \ldots, \frac{(2l-1)\pi}{l}$ and the number densities N(zj,t)'s are defined at $z_j = \frac{\pi}{2l}, \frac{3\pi}{2l}, \ldots, \frac{(4l-1)\pi}{2l}$. The above representations for u and N are put in (5.1.1) and a set of ordinary differential equations (ODE) is obtained for u(xj,t) and N(xj,t). These ODE's are then integrated numerically by using the fifth order implicit Adam-Moulton method. The nonlinear system is solved by using the Newton-Rapson method.

The power contained in the velocity fluctuations is given by

$$|u(t)|^2 = \sum_{k=-l}^{l-1} |\hat{u}_k|^2 , \qquad (5.2.2)$$

and similarly the power contained in the number density fluctuations is

$$|N(t)|^2 = \sum_{k=-l}^{l-1} |\hat{N}_k|^2. \qquad (5.2.3)$$

The computational domain is periodic. Moreover, the use of exponentials as interpolation functions allows us to obtain the integral term in (5.1.1) exactly:

$$\phi(z_j,t) = 1 - \varepsilon = \int_{-R}^{R} N(z+\xi,t)\, \pi(R^2 - \xi^2)\, d\xi$$

$$= \int_{-R}^{R} \Big[\sum_{k=-l}^{l-1} \hat{N}_k(t) e^{ik(\xi+z_j)} \pi(R^2-\xi^2) \Big] d\xi$$

$$= \sum_{k=-l}^{l-1} \hat{N}_k(t)\, e^{ikz_j} \Big[\int_{-R}^{R} e^{ik\xi}\, \pi(R^2-\xi^2)\, d\xi \Big]$$

$$= \sum_{k=-l}^{l-1} \hat{N}_k(t)\, e^{ikz_j}\, \frac{4}{3}\pi R^3\, \Theta(kR)$$

$$= \frac{4}{3}\pi R^3 \sum_{k=-l}^{l-1} \Big[\Theta(kR)\, \hat{N}_k(t) \Big] e^{ikz_j}, \qquad (5.2.4)$$

where $\Theta(kR) = 3\,\Big[\frac{\sin kR}{(kR)^3} - \frac{\cos kR}{(kR)^2}\Big]$. We note that the sequence $\{\phi(z_j,t)\}$ is simply a discrete Fourier transform of $\{\Theta(kR))\,\hat{N}_k(t)\}$. The last term in (5.2.4) can be evaluated by using the Fast Fourier Transform (FFT). So for a discrete problem in a finite periodic domain the convolution of equation (5.1.1) leads to a spatial filter, Θ(kR), see figure 1. The spatial filter Θ(kR) is unique in some respects; it completely removes the wave numbers for which Θ(kR) is zero, significantly reduces the effect of the wave numbers which are close to these zeros, and the large wave numbers for which Θ(kR) is small are also filtered out from the spectrum of N. The dynamical significance of all these wave numbers is greatly reduced because the momentum equation depends on φ which is obtained from N by applying the filter Θ(kR).

In order to obtain a numerical scheme which is stable over a large period of time it is necessary that the numerical scheme used conserves $|N|^2$. When global interpolation functions are used to evaluate the derivatives one of the effects of truncation, finite l, is the generation of high frequency components [Canuto, Hussaini, Quarteroni and Zang]. Many alternatives are available to overcome this problem. One can apply a low pass filter, do derivative filtering using many different types of filters available and/or add some artificial diffusion to stabilize the numerical scheme. But all these methods suffer from the fact that they modify the equation conserving N in a non-physical way. The method we use is based on obtaining the correct flux balance using the inflow and outflow. For this reason the grids for N and u are staggered.

5.3 Lagrangian quantities

One clear advantage any numerical simulation of the fluid flow has over an actual fluid flow experiment is that numerically one can obtain the Lagrangian quantities with relative ease. In fact in an experiment it is often impossible to obtain Lagrangian quantities. The Lagrangian quantities are very important when one is studying the rate of diffusion or the rate of mixing. For a tracer particle we obtain its position, the velocity and the acceleration as a function of time. We also obtain the local velocity gradients for the tracer particle.

5.4 Results

When we integrate (5.1.4) numerically we find that the numerical solution changes continuously with time and does not reach any fixed shape or form. One way to study this problem is to look at it as an initial value problem: we integrate the system of equations by assuming some initial conditions and some parameter values until the power contained in the fluctuations reaches some constant level. When the fluctuations from the uniform state are small, different modes grow until the nonlinear terms become comparable in magnitude to the linear terms. The nonlinear terms in our case act so as to stop the growth of the fluctuations; that is the power contained in the fluctuations remains bounded. In figure 4 we have plotted the power contained in the area fraction of solids and the velocity fluctuations as a function of time for two different initial conditions. In the first case the power contained in the fluctuations is small and in the second case it is large, and in both cases the spatial distribution for N and u fields is random at start. In the first case the power contained in the fluctuations grows with time until it reaches a level determined by the parameters and then that level is approximately maintained. In the second case the fluctuations lose power with time until the power is down to the same approximate level as in the first case, and again, this level is then approximately maintained. The form of the power spectrum for the two cases is also similar. This results holds for both N and u. This shows that the power spectrum of the final bounded solution is independent of the initial conditions. Bounded solutions of (5.1.4) can be decomposed into two parts, the uniform state and the fluctuations. The power contained in the fluctuating part remains bounded and has a well defined mean which is solely determined by the parameters Σ_m, n and ϕ_0. For fixed n and ϕ_0 the power contained in the fluctuating part is a monotonically increasing function of Σ_m. The results of the numerical simulations are shown in figure 5 and table 1. For a given n and ϕ_0 there is a maximum value of Σ_m for which a bounded solution exists, and for Σ_m larger than this there is no bounded solution. For n=4.8 and ϕ_0, the largest value of Σ_m for which a bounded solution can be obtained is 0.93. Bounded solutions of (5.1.4) are very complicated and chaotic. Only the statistical nature of these bounded solutions is described here. The numerical solution is two-dimensional, in space and time. The temporal variation of the area fraction at a point is chaotic, see figure 6. The spatial distribution of the area fraction contains all wave numbers. The large

wave numbers contain small energy, and the neutral modes given by the linear theory also contain small energy (see figure 5). All this is consistent with the experimental observations reported by Singh and Joseph [1991].

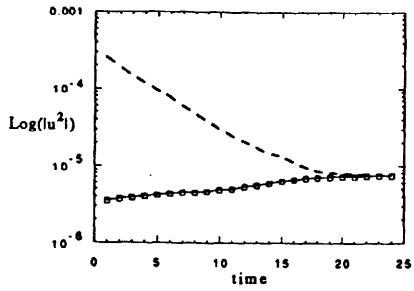

(a)

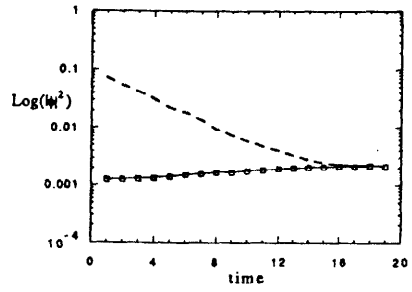

(b)

Fig. 4. The power contained in the fluctuations of the area fraction (a) of solids and the velocity (b) is plotted as a function of time for two different initial conditions.

$n = 4.8, \quad \phi_0 = 0.3.$

Σ_m	$\frac{\phi}{\phi_0}$	$\lvert \phi \rvert^2$	$\lvert u \rvert^2$
0.758	0.860	5.966	1.702
0.337	0.597	2.892	0.4109
0.0958	0.261	0.3161	1.19 e-2
0.0374	0.119	0.0492	7.09 e-4
0.0094	0.031	0.0021	7.47 e-6

Table 1. The power contained in the fluctuations of the area fraction of solids and the velocity, and the maximum area fraction of solids fluctuation for bounded solutions obtained for different Σ_m values are tabulated.

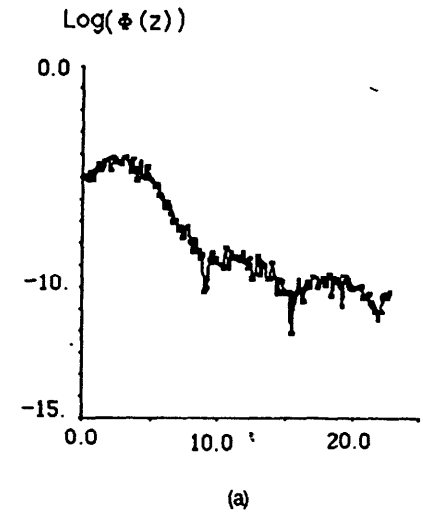

(a)

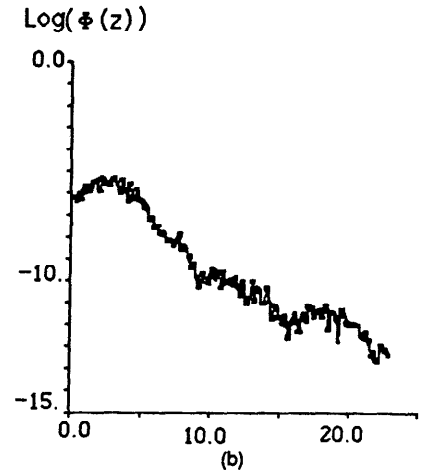

(b)

Fig. 5. For Σ_m = 0.0094, the power spectrum of bounded solution is shown. The blocked modes have very little power. (a) Area fraction of solids, (b) Velocity.

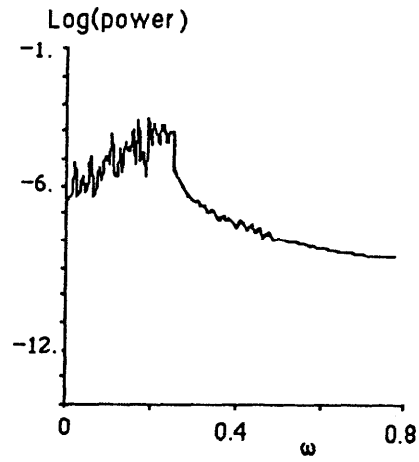

Fig. 6. The power spectrum of the area fraction of solids at a point is shown. It contains a band of large power, which implies that the voidage fluctuations are chaotic.

In a real fluidized bed there are always some fluctuation; particles move around and the area fraction of solids fluctuates. The magnitude of these fluctuations depends on the parameters of the bed under consideration. For application purposes one wants these fluctuations to be small because then the heat and mass transfer rates are maximum. The judgement whether the fluctuations are small enough or not is usually arrived at by looking at the spatial distribution of the particles and their motion. Now we will try to establish some connection between the numerical solutions obtained and a real fluidized bed. As we have stated before, when Σ_m is small the area fraction fluctuations are small and so the bed looks uniform. For a somewhat larger Σ_m the area fraction fluctuations are larger and the bed does not look that uniform, and for a still larger value of Σ_m the fluctuations are big enough to produce regions where the area fraction solids is very small. From a physical point of view this means as Σ_m becomes larger the ability of the system to distribute particles uniformly throughout the bed diminishes. Also, whenever there is a fluctuation in the area fraction, the particles experience an unbalanced force and accelerate. If in a region the fluctuation is such that the local area fraction is larger than the average then the particles experience more drag and accelerate upwards. Similarly, in the regions where the area fraction is smaller the particles fall downwards. Clearly, the acceleration force acting on a particle and its final speed is determined by the magnitude of the area fraction of solids fluctuation. But the magnitude of these fluctuations is in turn determined by Σ_m. In a nut-shell both the velocity fluctuations and the area fraction of solids fluctuations are determined by Σ_m. This can also be seen in table 1. It is interesting to write Σ_m as follows

$$\Sigma_m = \frac{2.17\, n^2 \phi_0}{\varepsilon_0^2} \frac{u_c^2}{D\tilde{g}}$$

$$= 6.94 \frac{C_1^2}{C_2^2}, \qquad (5.4.1)$$

where $C_1 = \frac{nu_c\phi_0}{\varepsilon_0}$ and $C_2^2 = 3.2\, \phi_0 \tilde{g} D$ are the kinematic and dynamic wave speeds proposed by Foscolo and Gibilaro. They also propose the following criterion for the stability

$$C_2 > C_1.$$

Or

$$\frac{C_2^2}{C_1^2} > 1. \qquad (5.4.2)$$

This criterion has been used successfully by then to predict the onset bubbling. Using (5.4.1) we can write this criterion in terms of Σ_m

$$\frac{6.94}{\Sigma_m} > 1 \quad \text{or} \quad \Sigma_m < 6.94. \qquad (5.4.3)$$

So the Foscolo-Gibilaro criterion predicts bubbling if Σ_m is larger than 6.94. As we have stated before the numerical solution blows up if Σ_m is larger than 0.93. One must note the remarkable similarity between the two, but at the same time we must remember that we are comparing two different things. The nonlinear numerical solution blows up when the particle distribution becomes too uneven, whereas the criterion for bubbling arises in the linear Foscolo-Gibilaro theory when the kinematic wave speed becomes larger than the dynamic wave speed. The numerical solution blows up much earlier, but the factor by which it is off is a constant and does not change. One last point is that as Σ_m increases the wave numbers which carry the maximum power become smaller. This was also observed in the experiments described by Singh and Joseph [1991].

The power spectrum of the Lagrangian velocity, position and acceleration is broad banded (see figure 7). This implies, the particle motion is chaotic. One way to understand the chaotic dynamics of a large dimensional dynamical system is to look at its projection in a phase space of much smaller dimension. In order to see any structure a judicious selection of such a sub space is very crucial. In figure 8 we show the trajectories in several such phase spaces. The trajectories for all these cases are bounded and stay close to the origin of the plot, the origin corresponds to the uniform state. For small Σ_m all trajectories are quite close to the origin, but for a larger Σ_m the trajectories wander around farther away from the origin. The basic nature of the phase portrait for all these cases is the same, the trajectories go around the origin and the time taken for one rotation varies from rotation to rotation. Now we look at our system in the phase space spanned by the particle acceleration and the local velocity gradient. These phase portraits are shown in figure 9. In this phase space the nature of the phase portraits changes with Σ_m. When Σ_m is small, the trajectories do not have any well defined structure. As Σ_m is increased two distinct oval shaped regions emerge, one in the second quadrant and the other in the fourth quadrant and the phase portraits become more structured. From this figure we note that for a large Σ_m, when $\frac{\partial u}{\partial z}$ is positive the acceleration is negative, and vice versa. The fractal (capacity) dimensions for the particle accelerations are shown in table 2. We note that for a larger Σ_m the capacity dimension is smaller, which means the particle path is less chaotic for a larger Σ_m.

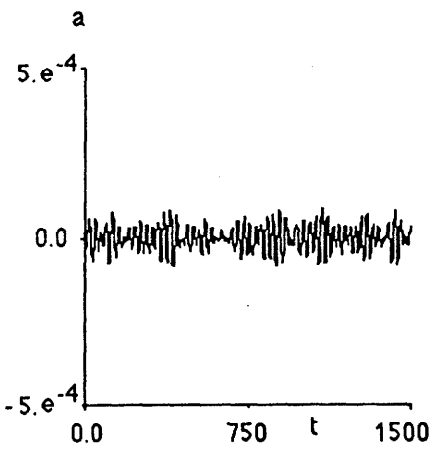

(a)

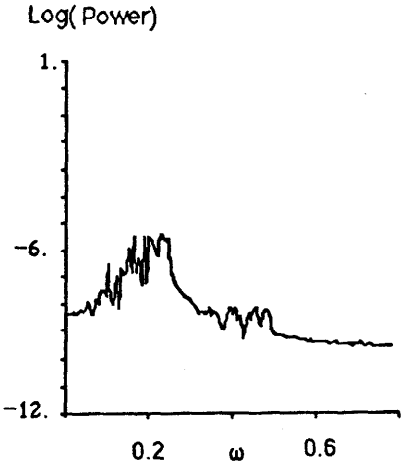

(b)

Fig. 7. The Lagrangian acceleration a for $\Sigma_m = 0.0094$. (a) a is plotted as a function of time. (b) its power spectrum. The power spectrum is broad banded, hence the particle motion is chaotic.

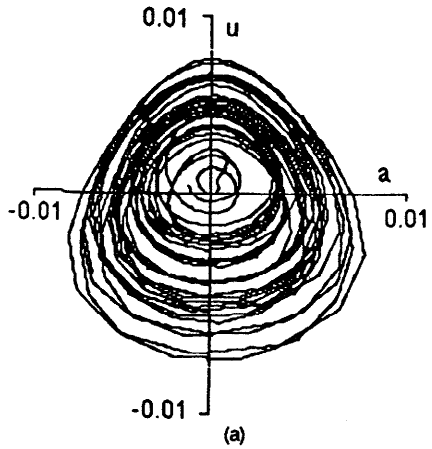

(a)

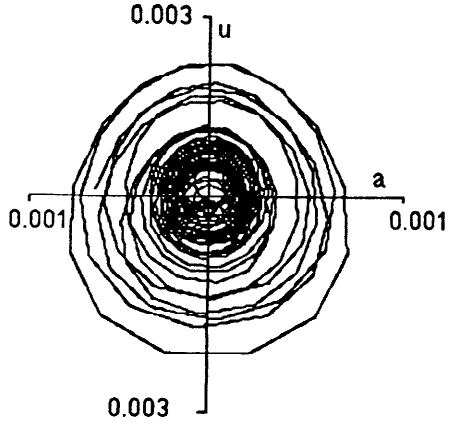

(b)

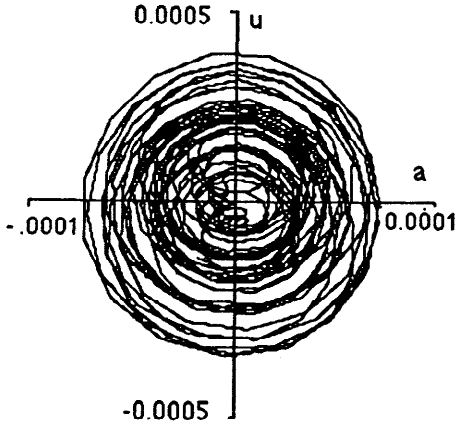

(c)

Fig. 8. The velocity u and the acceleration a are plotted with time as a parameter. (a) $\Sigma_m = 0.0094$, (b) $\Sigma_m = 0.0374$, (c) $\Sigma_m = 0.0958$. The trajectories go around the origin, the time taken for one rotation varies. For a larger Σ_m the trajectories wander farther away from the origin.

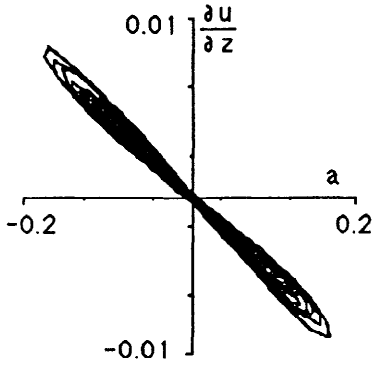

(a)

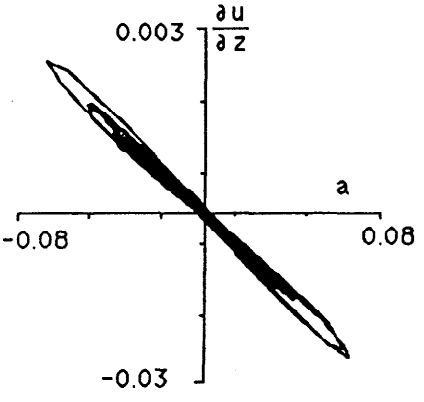

(b)

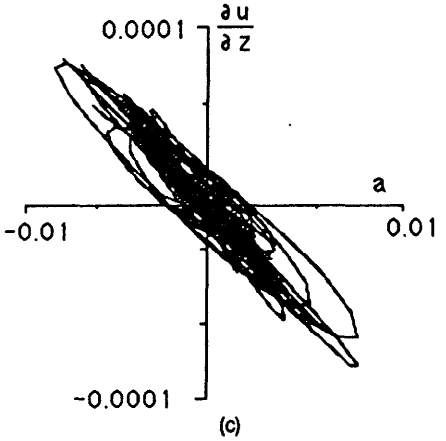

(c)

Fig. 9. $\frac{\partial u}{\partial z}$ is plotted against the acceleration a with time as a parameter. (a) $\Sigma_m = 0.0094$, (b) $\Sigma_m = 0.0374$, (c) $\Sigma_m = 0.0958$. The trajectories do not have a well defined structure when Σ_m is small. For a larger Σ_m there are two oval shaped regions, one in the second quadrant and the other in the fourth quadrant and the trajectory moves between

them. Also, for a larger Σ_m the trajectories wander farther away from the origin.

$n = 4.8, \quad \phi_0 = 0.3.$

Case	Σ_m	D
1	0.0958	1.700
2	0.0374	1.759
3	0.0094	1.813

Table 2. The fractal (capacity) dimension is tabulated for different Σ_m values. The fractal dimension decreases with Σ_m.

6. EXPERIMENTS

Singh and Joseph [1990] made video recordings of experiments on beds of fluidized spheres confined to move in two dimensions between glass plates. Analysis of the digitized signals gives the area fraction of solids as a function of space and time at a discrete set of points. The amplitude of the measured spectra is a strong function of frequency and wave number with deep minima at the blocked wave numbers predicted by stability theory and the numerical integration of the initial value problem. At low Reynolds numbers, the measured spectrum looks like the growth rate function from linear theory. As the Reynolds number increases, the graph of the power spectrum gets higher energy at smaller wave numbers, consistent with the increasing importance of wake effects.

In Figure 10 we have compared plots of the logarithm of the growth rate log(Reσ), (a), from linear theory as a function of αD with the magnitude logΦ of the power spectrum from nonlinear theory, (b), and experiments, (c). The blocked values of αD are evident in all cases. Many more and different comparisons of theory and experiments are discussed by Singh and Joseph [1990] with similar agreements. We think that the agreements between the predictions of the simple theory with finite size but no gradient are astonishing, since there are no disposable constants and nothing has been adjusted. On the other hand, the predictions of the gradient theory do not agree with the experiments on two-dimensional fluidizations.

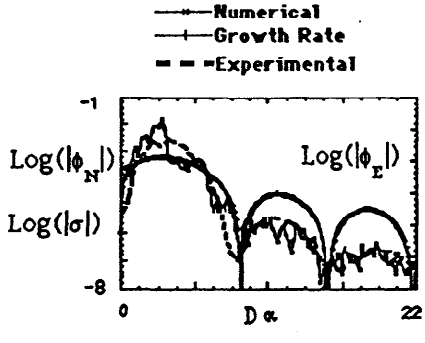

Fig. 10: Comparison of log|σ|, log $|\phi_N|$ and log$|\phi_E|$, where σ is the growth rate of the linear theory of stability of uniform fluidization, log $|\phi_N|$ is the amplitude of the power spectrum computed numerically for the three variable nonlinear theory and log$|\phi_E|$ where ϕ_E is the power spectrum measured in the experiments. The value of the parameter Σ_m which we estimated for the experiments is 1.79. For the nonlinear numerical solution Σ_m is 0.0958. The amplitude is a strong function of Σ_m, but the blocked wave numbers are robust, independent of sphere size or Reynolds number.

7. CONCLUSIONS

- If the finite size of particles is accounted then the zeroth order problem is not Hadamard unstable; that is, the finite size of particles is a regularizer.

- We integrate the problem governed by the zeroth order theory as an initial value problem and find that bounded solutions with nearly stationary power exist when Σ_m is small, and no such solution exist when Σ_m is large. The power spectrum of bounded solution contains low power for the blocked wave numbers and looks similar to the power spectrum of the experimental data and the growth rate plot of the zeroth order theory (see figure 10).

- Both experimental and numerical results show that uniform fluidization is unstable.

- The experimental data and the data obtained numerically show that the fluctuations at a point are chaotic.

- The particle paths computed using the nonlinear zeroth order theory are chaotic, and as Σ_m is decreased they become more chaotic.

This research was supported under grants from the National Science Foundation, the US Army Research Office, Mathematics, the Department of Energy, and the Supercomputer Institute of the University of Minnesota.

REFERENCES

Batchelor, G.K., 1988, "A new theory of the instability of a uniform fluidized bed," *J. Fluid Mech.* vol 193, pp 75-110.

Canuto, C., Hussaini, M.Y., Quarteroni, A. and Zang, T.A. 1988, "Spectral methods in fluid dynamics," Springer-Verlag.

Foscolo, P.V. and Gibilaro, L.G., 1987, "Fluid dynamic stability of fluidized suspensions. The particle bed model," *Chem Eng Sci.*, vol 42, pp 1489-1500.

Joseph D. D. 1990, "Generalization of Foscolo-Gibilaro analysis of dynamic waves," *Chem Eng Sci.*, vol 45, 411-414.

Singh P. and Joseph, D. D. 1990, "One-dimensional, particle bed models of fluidized suspensions," *Two phase flows in fluidized beds, sedimentation and granular flows. IMA volumes in Mathematics and its Applications 26,* Springer-Verlag.

Singh P. and Joseph, D. D. 1991, "Chaos and structure in two-dimensional beds of spheres fluidized by water," (Submitted for publication in JFM)

Volpicelli, G., Massimilla, L. and Zenz F.A. 1966, "Non-homogeneties in solid-liquid fluidization," *Chem. Eng. Symp. Series*, vol 67, pp 42-50.